Received: 2 October 2019 | Revised: 4 March 2020 | Accepted: 16 March 2020

DOI: 10.1002/sia.6783

ECASIA SPECIAL ISSUE PAPER

SURFACE and INTERFACE ANALYSIS WILEY

X-ray and UV photoelectron spectroscopy of Ag nanoclusters

Eleonora Bolli[1,2] | Alessio Mezzi[1] | Luca Burratti[2] | Paolo Prosposito[2] | Stefano Casciardi[3] | Saulius Kaciulis[1]

[1]Institute for the Study of Nanostructured Materials, ISMN-CNR, Rome, Italy

[2]Department of Industrial Engineering, University of Rome Tor Vergata, Rome, Italy

[3]Department of Occupational and Environmental Medicine, Epidemiology and Hygiene, National Institute for Insurance against Accidents at Work (INAIL), Rome, Italy

Correspondence
Eleonora Bolli, Institute for the Study of Nanostructured Materials, ISMN-CNR, 00015 Rome, Italy.
Email: eleonora.bolli@ismn.cnr.it

The main purpose of the present work is to analyze a series of Ag nanoparticles (NPs) with different size or ligand functionalization by using X-ray photoelectron spectroscopy (XPS) and to identify the differences in the band-shape and energy peak position of photoemission spectra due to the particle dimension. A transmission electron microscopy characterization was performed, to verify the consistency of the results. Three types of samples were prepared starting from $AgNO_3$ water solution and adding different capping agents. In the first two cases, the formation of NPs was promoted by the reduction of silver ions Ag^{+1} to metallic Ag^0 through the addition of sodium borohydride, whereas in the last case, it was triggered by the exposure to UV light. Depending on the size of the NPs, a different physical behavior can be recognized. NPs with diameter of about 5 nm are characterized by the phenomenon of localized surface plasmon resonance (LSPR). The other type of samples having a diameter of about 1.5 nm presents discrete energy levels instead of electronic bands, and in this case, a typical fluorescence phenomenon can be observed. In the latter case, we can refer to such systems as nanoclusters. The XPS analyses were focused on the Ag 3D spectra looking for the possible shifts of the Ag doublet as a function of the particles size. The ultraviolet photoelectron spectroscopy with He II source was used for the investigation of possible changes in the valence band.

KEYWORDS

Ag nanoclusters, Ag nanoparticles, TEM, UPS, XPS

1 | INTRODUCTION

In the last decade, nanomaterials have attracted the attention of scientific community for their unusual features with respect to the same bulk material. They present interesting and innovative properties related to the small dimensions that allow their use in many fields such as biology, material science, physics, energy, and medicine with a huge number of applications,[1–3] spanning from energy to sensors and from bio-labeling to drug delivery and personalized medicine. Among the most studied nanomaterials, there are metal nanoparticles (NPs) and nanoclusters (NCs) with a mean diameter above and below 2 nm, respectively. The partial or total confinement of electrons in these two types of nanomaterials confer them very interesting physical and chemical properties. Optical features are probably the most studied for the ease of measurement and for their use in numerous fields of applications such as biomedicine,[4,5] biotechnology,[6,7] energy,[8–10] optics, and optoelectronics.[11–18]

Silver NPs (Ag NPs) represent an example of noble metal NPs with peculiar properties, according to the principle for which the material properties can change as a function of its size. It is well known that bulk Ag is a good electrical and thermal conductor and has a highly reflective surface. However, the reduced size ($d \leq 100$ nm) of Ag NPs allows the phenomenon of localized surface plasmon resonance (LSPR)[19] or quantum effects, like photoluminescence (PL), if the size approaches the dimension of 2 nm.[20]

In X-ray photoelectron spectroscopy (XPS), the metallic Ag $3D_{5/2}$ peak lies at a binding energy (BE) of 368.2 eV and has a very small

chemical shift; therefore, the identification of oxidation state in bulk Ag compounds is difficult. An interesting question on this regard is: could this property change if the NPs dimensions decrease? Numerous papers confirm this effect (e.g., Lopez-Salido et al,[21]) but a systematic knowledge of the properties of Ag NPs as a function of their dimension is still lacking.

In this work, we report a detailed XPS study on a series of three Ag samples with reduced size: small Ag NPs with dimension of about 5 nm and two types of silver nanoclusters (Ag NCs) with a different size (<2 nm) and capping agent. A shift to higher BE and a broadening of Ag 3D spin-orbit doublets as a function of the sample dimension was revealed. The size and morphology of NPs was carefully determined by means of transmission electron microscopy (TEM). Moreover, in order to obtain more information about Ag nanomaterials, ultraviolet photoelectron spectroscopy (UPS) was carried out and Auger parameters and valence band spectra were determined.

2 | EXPERIMENTAL

2.1 | Sample preparation

Silver nitrate ($AgNO_3$), sodium 3-mercapto-1-propanesulfonate (3MPS), poly(methacrylic acid, sodium salt) water solution (average M_w ~9500, 30 wt.% in H_2O) (PMAA), lipoic acid (LA), sodium borohydride ($NaBH_4$), sodium hydroxide (NaOH), and nitric acid (HNO_3) were purchased from Sigma Aldrich. All chemical reagents have been used without further purification processes. All reagents were dissolved in deionized Milli-Q water.

The first type of system is Ag NPs + 3MPS. NPs were synthesized by reducing $AgNO_3$ with $NaBH_4$ under vigorous stirring at the temperature of 3°C. The thiol (3MPS) was subsequently added for the capping of NPs, accordingly to previous work.[22]

The second type of system is Ag NCs + PMAA; in this case, the structures were synthesized starting from $AgNO_3$ water solution and PMAA as a capping agent, following the synthesis reported in a recent work.[23] The Ag^+ solution was mixed with the PMAA solution, and the pH was adjusted to 4 by adding HNO_3. To promote the reduction reaction of Ag ions to metal, the mixture was exposed to UV lamp (300 W, NEWPORT, Oriel Instruments, USA) for 6 min, whereas nitrogen gas was fluxed on the solution surface during UV exposition to hamper the oxidation of the growing Ag NCs.

The last type of particles is Ag NCs + LA. In a typical LA synthesis, 78 mg of lipoic acid was solved in 30 ml of NaOH/water solution (6 ml of NaOH and 24 ml of deionized water), then 1.5 ml of $AgNO_3$ water solution (4.2 mg/ml) was added drop-wise to LA solution under vigorous stirring. Afterwards, 3 ml of $NaBH_4$ water solution (4.2 mg/ml) was added dropwise to the previous mixture, maintaining vigorous stirring. The mechanical stirring was continued for 2 h.

2.2 | Surface analyses

The samples for surface analyses were prepared by depositing a drop of water solution of each sample on Au foil (purity 99.99%) for XPS and on Si/SiO_2 substrate for UPS, then they were dried in air at 80°C by using a heating plate. The support of Au foil was used in order to avoid the possible sample charging under X-rays, whereas Si/SiO_2 substrate without signal interference close to the Fermi level was better suited for the valence band spectra.

XPS analyses were carried out by using a spectrometer Escalab 250Xi (Thermo Fisher Scientific, UK) equipped with a monochromatized Al Kα X-ray source (1486.6 eV), high intensity He UV source and six channeltron detector. The valence band was investigated by XPS (with Al Kα radiation) and UPS with He II (40.8 eV) radiation at high photon flux (>1.5×10^{10} photons per second). All XPS spectra were acquired at pass energy of 40 eV and standard electromagnetic lens mode corresponding to analyzed surface area of ~1 mm in diameter. The absence of sample charging was controlled by monitoring the position of C 1 s peak from aliphatic carbon at BE = 285.0 eV and the Fermi level in the valence band at BE = 0 eV. The pressure in the main chamber during the XPS acquisition was maintained at ~2×10^{-9} mbar, whereas during UPS measurements, it was increased to 2×10^{-8} mbar for He II source. All experimental data were processed using Avantage v.5 software.

2.3 | Transmission electron microscopy

The morphological characterization of the Ag NPs and Ag NCs have been carried out in a TEM apparatus FEI TECNAI 12 G2 (Thermo Fisher Scientific Ltd., UK) equipped with an energy filter (GATAN Biofilter model GIF) and Peltier cooled SSC (slow scan charged coupled device) multiscan camera (794 IF model).

3 | RESULTS AND DISCUSSION

3.1 | Morphological characterization

TEM results for the sample Ag NPs + 3MPS are reported in Figure 1: (A) typical image of NPs and (B) diameter dispersion calculated for about 400 particles. The mean diameter determined with this procedure was equal to 3.9 ± 0.8 nm.

TEM image of the sample Ag NCs + PMAA is shown in Figure 2. The NCs are clearly visible, and their size and density are noticeably smaller than those of NPs. In this sample, the same statistical approach applied previously on about 100 particles gave a mean diameter of 1.9 ± 0.8 nm.[24]

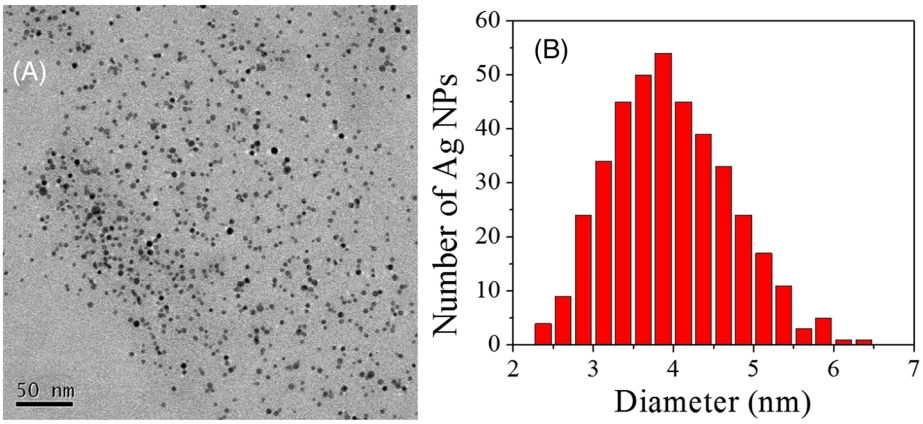

FIGURE 1 (A) TEM image of Ag NPs + 3MPS; (B) graph of NPs diameter dispersion

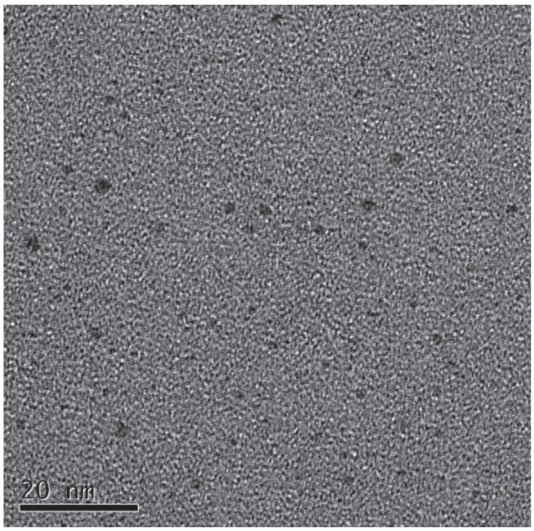

FIGURE 2 TEM image of Ag NCs stabilized by PMAA

3.2 | X-ray photoelectron spectroscopy/ultraviolet photoelectron spectroscopy

The spectra of Ag 3D spin-orbit doublets measured by XPS for Ag NPs, Ag NCs, and silver foil reference are shown in Figure 3. The experimental data are represented by light blue circles, whereas the results of peak fitting are represented by black lines. The components of bulk metallic Ag and shifted Ag are indicated with red and blue lines, respectively. The spectra were subjected to two different phenomena: the first one is a shift to higher binding energy (BE), when the dimension of the particles is reduced, and the second one is an increase of the full width at half maximum (FWHM) for smaller particles. For all the nanoparticle systems investigated, the Ag 3D spectra are composed of one or two different components with atomic % reported in Figure 4.

The Ag $3D_{5/2}$ spectrum of Ag NPs + 3MPS is reported in Figure 3B, and it is composed by only metallic silver peak at BE = 368.2 eV. The FWHM of this peak was of 1.1 eV; that is, the whole Ag 3D spectrum was identical to the one of bulk Ag foil (see Figure 3A). Instead, for the sample of Ag NCs + PMAA reported in Figure 3c, the Ag $3D_{5/2}$ spectrum can be divided into two

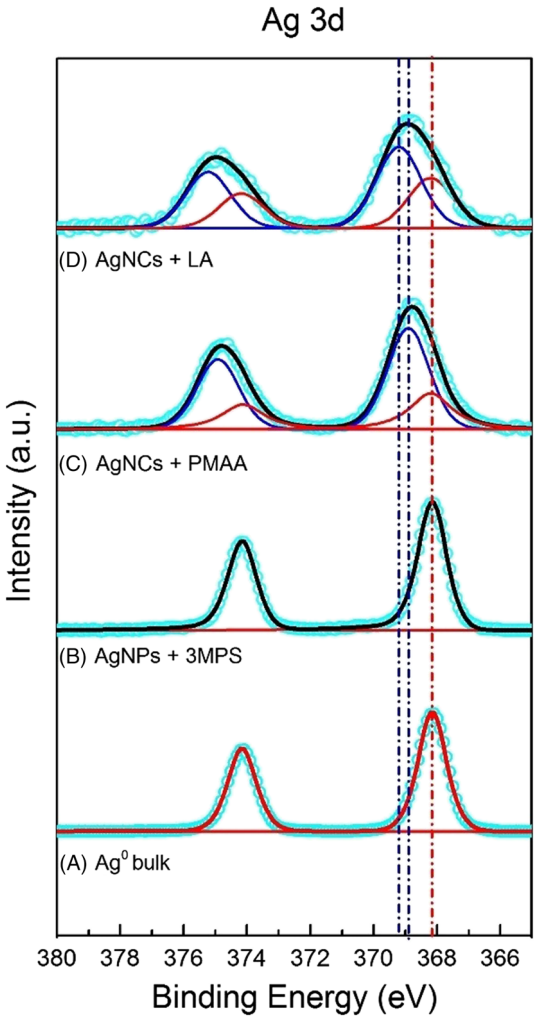

FIGURE 3 Comparison of the Ag 3D spectra of the investigated samples: (A) bulk Ag foil; (B) Ag NPs + 3MPS; (C) Ag NCs + PMAA; (D) Ag NCs + LA

components with FWHMs of 1.6 eV; in this case, the content of metallic Ag is much smaller than the second one at BE = 368.9 eV, which could be attributed to the presence of very small Ag NPs. Because the size of Ag NCs is much smaller than the one of NPs, this result is in good agreement with the size shift model,[21] where the BE value is increasing as the nanoparticle size decreases.

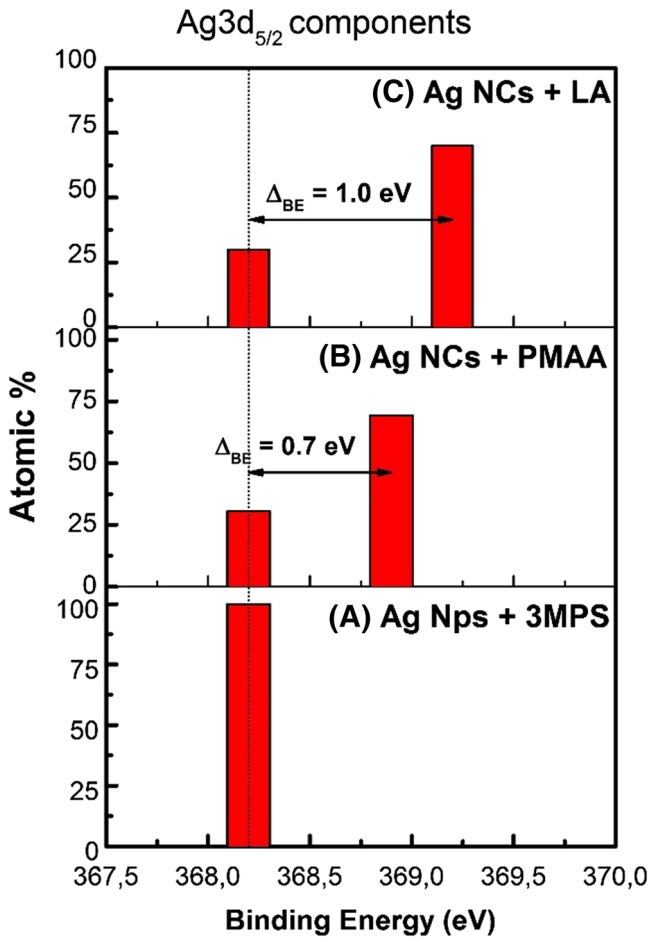

FIGURE 4 Atomic % of Ag $3D_{5/2}$ components for the (A) Ag NPs + 3MPS system, (B) Ag NCs + PMAA, and (C) Ag NCs + LA

Figure 3D shows the Ag 3D spectra for Ag NCs + LA. This sample exhibits the greatest Ag $3D_{5/2}$ peak shift; thus, it is supposed to be the system with the smallest particles. In this sample, a peak at BE = 369.2 eV with FWHM of 1.6 eV was revealed in addition to the lower peak of metallic Ag. It seems that the width of Ag 3D peaks is slightly increasing, when the particles decrease in size. This phenomenon can be attributed to the life time of excited state in the XPS measurements or to a greater dispersion of the particle size.[25]

As it was emphasized above, a maximum shift of 1.0 eV to higher BE and the peak broadening by 0.5 eV was observed for Ag $3D_{5/2}$ core level in the samples with the smallest clusters. The summary of BE shift is plotted as a function of particles size in Figure 5, which is in a good agreement with literature data.[21]

The peak maximum of X-rays induced Auger transition Ag $M_4N_{45}N_{45}$ was registered at kinetic energy KE = 357.3 eV for the sample Ag NPs + 3MPS. Taking into account the BE value of Ag $3D_{5/2}$ peak of the same sample (BE = 368.2 eV), the calculated Auger parameter is equal to 725.5 eV; that is, it is very close to the Auger parameter of bulk Ag metal reported in literature (726.0 eV).[26] In the same way, the Auger parameters for the other two systems equal to 724.4 eV and 723.9 eV for the Ag NCs + PMAA and the Ag NCs + LA, respectively, have been calculated. These values are lower than the

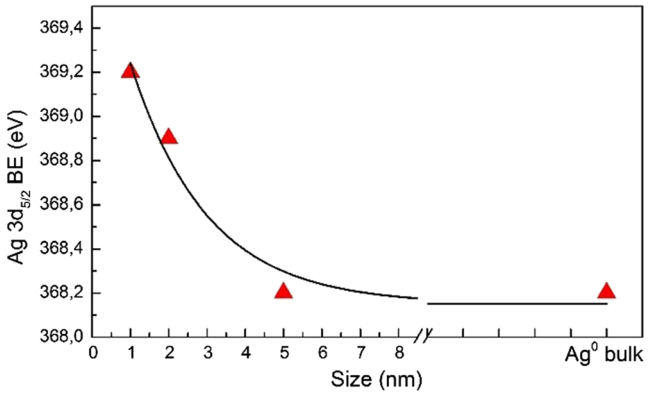

FIGURE 5 Plot of BE of Ag $3D_{5/2}$ component as a function of particles size

Auger parameter of metallic Ag, and they are close to that of Ag_2O (724.3 eV).[26] However, a lower value of the Auger parameter for Ag nanoclusters has been already reported in literature.[27,28]

The spectra of the valence band acquired for different samples by using XPS and UPS (with He II source) are presented in Figures 6A and 6B, respectively. When the aqueous solution of Ag particles dries on a solid substrate, it is expected to obtain an overlayer of NPs covered by the residue of capping agent; therefore, the valence band spectra can be strongly influenced by the coverage with 3MPS, PMAA, and LA. The thickness of this coverage can be higher than the UPS information depth, resulting in the valence spectra only of the

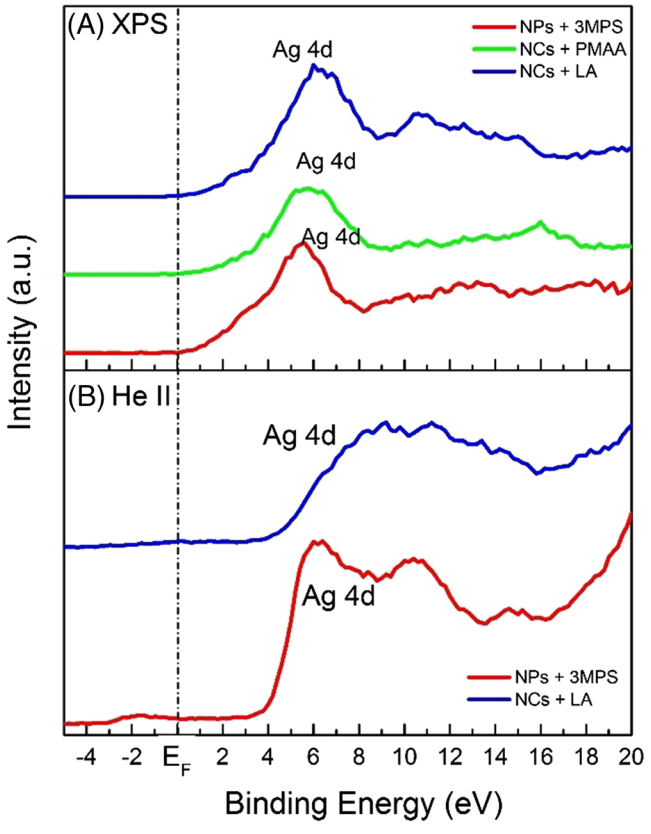

FIGURE 6 Comparison of the valence band spectra acquired for investigated samples by using (A) X-ray source and (B) He II source

capping agents. For this reason, all the samples were dried at 80°C, inducing the fast evaporation of solvent and capping agents. The signal of Ag 4D at about 5 eV is clearly visible in all XPS and UPS spectra, except of the sample Ag NCs + PMAA, where the residue of PMAA was too thick for UPS, but the signal of Ag 4D is present in XPS due to its higher information depth. In the sample Ag NPs + 3MPS, where from XPS results was revealed only the presence of metallic Ag, the shape of Ag 4D signal in the UPS valence band spectrum is similar to the one of bulk Ag metal reported in literature.[29]

3.3 | Application for sensors

Recently, many sensors based on different nanosized materials have been developed, achieving a high sensitivity and selectivity for heavy metal ions.[29–39] Metal NP systems, for example, exhibit a pronounced LSPR effect, and this optical property can be monitored also in the presence of various types of contaminants, such as heavy metal ions.[19,23] In general, three parameters can change due to the contamination: energy peak position (maximum of the LSPR band), FWHM, and the band intensity. The peak shift towards red range of visible spectrum is often related to aggregation of NPs caused by the presence of specific metal ions. This type of optical sensors is already used to detect Co(2+) and Ni(2+) ions in water.[14,19,22]

The absorption spectra of Ag NPs-3MPS without (reference solution) and with 5 ppm of Ni(2+) are shown in Figure 7. The plasmonic band of the reference sample changes the peak position (red shift), the intensity, and FWHM. In this case, we reported a linear behavior of the energy peak as a function of the contaminant in the range from 0.3 to 1 ppm.[22]

Another optical property, which is even more sensible to a change of the surrounding medium is the PL emission. As it was mentioned before, metal NCs exhibit this optical feature, which can be used to detect easily and rapidly the presence of pollutants.[3,35,37] In general, the peak position and intensity can change due to the presence of heavy metal ions. Exploiting the PL emission of Ag NCs, we have developed a sensor able to detect the lead ions in potable water near the legal limit,[23] established by the World Health Organization. Typical response of this sensor is reported in Figure 8, where the intensity of PL emission is enhanced by the presence of Pb(2+).

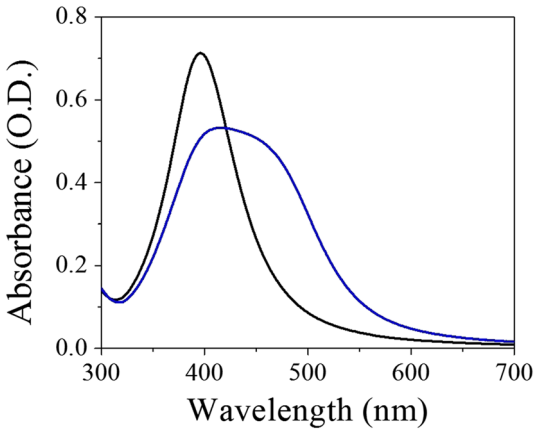

FIGURE 7 Absorption spectra of Ag NPs-3MPS in the UV–Vis range: Black line represents the reference sample, blue line represents the Ag NPs contaminated with 5 ppm of Ni(2+) ions

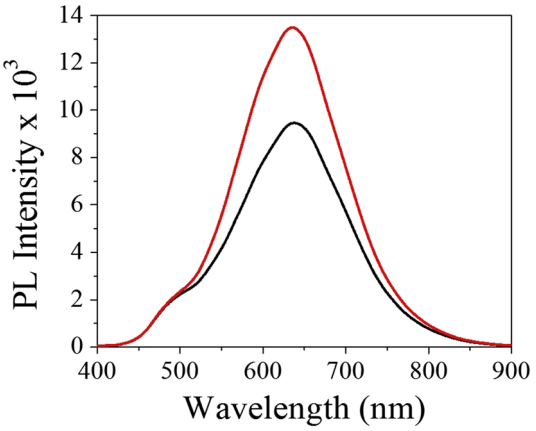

FIGURE 8 PL emission spectra of Ag NCs-PMAA in the absence (black line) and in presence of 50 μM of Pb(2+) ions (red curve)

4 | CONCLUSIONS

Ag NPs of different diameters in the range of 1.5–5 nm with different capping agents were synthesized. Obtained samples were characterized by means of different techniques, such as XPS, UPS, and TEM. A detailed analysis of the main photoemission peak of Ag 3D have been carried out, and the results were compared with a reference sample of bulk Ag metal. The changes in Ag 3D spectra were related to the particle dimensions: a shift to higher BE and an enlargement of the FWHMs with decreasing particles size was clearly observed.

The signal of Ag 4D was detected in all valence band spectra, except of the sample with PMAA, where the residual overlayer of capping agent was too thick for UPS. The presence of only metallic Ag state in the sample Ag NPs + 3MPS revealed by XPS was confirmed by the shape of Ag 4D signal in the UPS valence band spectrum.

The application of Ag NPs and NCs for optical detection of heavy metal ions (Ni and Pb) was demonstrated successfully.

ORCID

Eleonora Bolli https://orcid.org/0000-0002-6079-0900
Alessio Mezzi https://orcid.org/0000-0002-2887-520X
Saulius Kaciulis https://orcid.org/0000-0002-9868-7626

REFERENCES

1. Lamastra FR, De Angelis R, Antonucci A, et al. Polymer composite random lasers based on diatom frustules as scatterers. *RSC Adv*. 2014; 4(106):61809-61816.
2. Le Guével X, Palazzesi C, Prosposito P, Della Giustina G, Brusatin G. Influence of chelating agents on the photopolymerization of hybrid Ti-based waveguides. *J Mater Chem*. 2008;18(30):3556-3562.
3. Burratti L, De Matteis F, Casalboni M, Francini R, Pizzoferrato R, Prosposito P. Polystyrene photonic crystals as optical

sensors for volatile organic compounds. *Mater Chem Phys*. 2018;212:274-281.
4. Rai M, Ingle AP, Birla S, Yadav A, Santos CA. Strategic role of selected noble metal nanoparticles in medicine. *Rev Microbiol*. 2016;42:696-719.
5. Akhtar MS, Panwar J, Yun YS. Biogenic synthesis of metallic nanoparticles by plant extracts. *ACS Sustain Chem Eng*. 2013;1:591-602.
6. Edmundson MC, Capeness M. Exploring the potential of metallic nanoparticles within synthetic biology. *N Biotechnol*. 2014;31(6):572-578.
7. Zheng XT, Ananthanarayanan A, Luo KQ, Chen P. Glowing graphene quantum dots and carbon dots: properties, syntheses, and biological applications. *Small*. 2015;11(14):1620-1636.
8. Venditti I, Barbero N, Russo MV, et al. Electrodeposited ZnO with squaraine sentisizers as photoactive anode of DSCs. *Mater Res Express*. 2014;1(1):1-18.
9. Julien CM, Mauger A. Nanostructured MnO_2 as electrode materials for energy storage. *Nanomaterials*. 2017;7(11):396-396.
10. Barettin D, Di Carlo A, De Angelis R, Casalboni M, Prosposito P. Effect of dielectric Bragg grating nanostructuring on dye sensitized solar cells. *Opt Express*. 2012;20(23):A888-A897.
11. Yadav A, De Angelis R, Casalboni M, et al. Spectral properties of self-assembled polystyrene nanospheres photonic crystals doped with luminescent dyes. *Opt Mater*. 2013;35(8):1538-1543.
12. Ramírez-Herrera DE, Rodríguez-Velázquez E, Alatorre-Meda M, et al. NIR-emitting alloyed CdTeSe QDs and organic dye assemblies: a non-toxic, stable, and efficient FRET system. *Nanomaterials*. 2018;8(4):231–231.
13. Venditti I. Gold nanoparticles in photonic crystals applications: a review. *Dent Mater*. 2017;10(2):97-97.
14. Corsi P, Venditti I, Battocchio C, et al. Designing an optimal ion adsorber at the nanoscale: the unusual nucleation of AgNP/Co^{2+}–Ni^{2+} binary mixtures. *J Phys Chem C*. 2019;123(6):3855-3860.
15. Prosposito P, Casalboni M, Orsini E, Palazzesi C, Stella F. UV-nanoimprinting lithography of Bragg gratings on hybrid sol-gel based channel waveguides. *Solid State Sci*. 2010;12(11):1886-1889.
16. Li C, Chunying W. DNA-templated silver nanocluster as a label-free fluorescent probe for the highly sensitive and selective detection of mercury ions. *Sens Actuators B*. 2017;242:563-568.
17. Orsini A, Medaglia PG, Scarpellini D, Pizzoferrato R, Falconi C. Towards high-performance, low-cost quartz sensors with high-density, well-separated, vertically aligned ZnO nanowires by low-temperature, seed-less, single-step, double-sided growth. *Nanotechnology*. 2013;24(35):355503-355503.
18. Zaniewski AM, Schriver M, Lee JG, Crommie MF, Zettl A. Electronic and optical properties of metal-nanoparticle filled grapheme sandwiches. *Appl Phys Lett*. 2013;102(2):023108-023108.
19. Mochi F, Burratti L, Fratoddi I, et al. Plasmonic sensor based on interaction between silver nanoparticles and Ni^{2+} or Co^{2+} in water. *Nanomaterials*. 2018;8(7):488-488.
20. Burratti L, Bolli E, Casalboni M, et al. Synthesis of fluorescent Ag nanoclusters for sensing and imaging applications. *Mater Sci Forum*. 2018;941:2243-2248.
21. Lopez-Salido I, Lim DC, Kim YD. Ag nanoparticles on highly ordered pyrolytic graphite (HOPG) surfaces studied using STM and XPS. *Surf Sci*. 2005;588(1-3):6-18.
22. Prosposito P, Mochi F, Ciotta E, et al. Hydrophilic silver nanoparticles with tunable optical properties: application for the detection of heavy metals in water. *Beilstein Journal of Nanotechnology*. 2016;7:1654-1661.
23. Burratti L, Ciotta E, Bolli E, et al. Fluorescence enhancement induced by the interaction of silver nanoclusters with lead ions in water. *Colloids Surf A Physicochem Eng Asp*. 2019;579:123634-123634.
24. Burratti L, Ciotta E, Bolli E, et al. Synthesis of fluorescent silver nanoclusters with potential application for heavy metal ions detection in water. *IP Conf Proc*. 2019;2145:020007-020007.
25. Paszti Z, Peto G, Horvàth ZE, Karacs A, And GL. Electronic structure of Ag nanoparticles deposited on Si (100). *Solid State Commun*. 1998;107(7):329-333.
26. Vijay KK. XPS core level spectra and Auger parameters for some silver compounds. *J Electron Spectros Relat Phenom*. 1991;56:273-277.
27. Bukhtiyarov V, Yu A, Stakheev A, Mytareva I, Prosvirin P, Bukhtiyarova VI. In situ XPS study of the size effect in the interaction of NO with the surface of the model Ag/Al_2O_3/FeCrAl catalysts A. *Russ Chem Bull Int Ed*. 2015;64(12):2780-2785.
28. Han Y, Xu Q, Wang W, Zhu J. Atomic-scale insight into the metal −support interaction: a case for Ag nanoparticles on ordered ZrO_2(111) thin films. *J Phys Chem*. 2015;119:4235-4241.
29. Apai G, Lee S-T, Mason HG. Valence band formation in small silver clusters. *Solid State Commun*. 1981;37(3):213-217.
30. Barettin D, De Angelis R, Prosposito P, Auf der Maur M, Casalboni M, Pecchia A. Model of a realistic InP surface quantum dot extrapolated from atomic force microscopy results. *Nanotechnology*. 2014;25(19):195201-195201.
31. Pedrero M, Campuzano S, Pingarrón JM. Quantum dots as components of electrochemical sensing platforms for the detection of environmental and food pollutants: a review. *J AOAC Int*. 2017;100(4):950-961.
32. Bhattacharjee Y, Chatterjee D, Chakraborty A. Label-free cysteamine-capped silver nanoparticle-based colorimetric assay for Hg (II) detection in water with subnanomolar exactitude. *Sens Actuators B*. 2018;255:210-216.
33. Zheng P, Wu N. Fluorescence and sensing applications of graphene oxide and graphene quantum dots: a review. *Chem Asian J*. 2017;12(18):2343-2353.
34. Priyadarshini E, Pradhan N. Gold nanoparticles as efficient sensors in colorimetric detection of toxic metal ions: a review. *Sens Actuators B*. 2017;238:888-902.
35. Ciotta E, Paoloni S, Richetta M, et al. Sensitivity to heavy-metal ions of unfolded fullerene quantum dots. *Sensors*. 2017;17(11):2614-2614.
36. Mahmoud MA, O'Neil D, El-Sayed MA. Hollow and solid metallic nanoparticles in sensing and in nanocatalysis. *Chem Mater*. 2014;26(1):44-58.
37. De Angelis R, D'Amico L, Casalboni M, Hatami F, Masselink WT, Prosposito P. Photoluminescence sensitivity to methanol vapours of surface InP quantum dots: effect of dot size and coverage. *Sens Actuators B*. 2013;189:113-117.
38. Mou X, Wang J, Meng X, Liu J, Shi L, Sun L. Multifunctional nanoprobe based on upconversion nanoparticles for luminescent sensing and magnetic resonance imaging. *JOL*. 2017;190:16-22.
39. Piloto C, Mirri F, Bengio E, et al. Room temperature gas sensing properties of ultrathin carbon nanotube films by surfactant-free dip coating. *Sens Actuators B*. 2016;227:128-134.

How to cite this article: Bolli E, Mezzi A, Burratti L, Prosposito P, Casciardi S, Kaciulis S. X-ray and UV photoelectron spectroscopy of Ag nanoclusters. *Surf Interface Anal*. 2020;1–6. https://doi.org/10.1002/sia.6783